HYDROLOGICAL PROCESSES
Hydrol. Process. **24**, 1766–1780 (2010)
Published online 24 March 2010 in Wiley InterScience
(www.interscience.wiley.com) DOI: 10.1002/hyp.7613

The effect of soil type, meteorological forcing and slope gradient on the simulation of internal erosion processes at the local scale

Guillaume Nord[1]* and Michel Esteves[2]

[1] *Institute of Environmental Assessment and Water Research, CSIC, Solé i Sabarís s/n, 08028 Barcelona, Spain*
[2] *LTHE (Laboratoire d'Etude des Transferts en Hydrologie et Environnement), IRD, Université de Grenoble 1, CNRS, G-INP, BP 53, 38041 Grenoble Cedex 09, France*

Abstract:

Numerical simulation experiments of water erosion at the local scale (20×5 m) using a process-based model [Plot Soil Erosion Model_2D (PSEM_2D)] were carried out to test the effects of various environmental factors (soil type, meteorological forcing and slope gradient) on the runoff and erosion response and to determine the dominant processes that control the sediment yield at various slope lengths. The selected environmental factors corresponded to conditions for which the model had been fully tested beforehand. The use of a Green and Ampt model for infiltration explained the dominant role played by rainfall intensity in the runoff response. Sediment yield at the outlet of the simulated area was correlated positively with rainfall intensity and slope gradient, but was less sensitive to soil type. The relationship between sediment yield (soil loss per unit area) and slope length was greatly influenced by all environmental factors, but there was a general tendency towards higher sediment yield when the slope was longer. Contribution of rainfall erosion to gross erosion was dominant for all surfaces with slope lengths ranging from 4 to 20 m. The highest sediment yields corresponded to cases where flow erosion was activated. An increase in slope gradient resulted in flow detachment starting upstream. Sediment exported at the outlet of the simulated area came predominantly from the zone located near the outlet. The microrelief helped in the development of a rill network that controlled both the ratio between rainfall and flow erosion and the relationship between sediment yield and slope length. Copyright © 2010 John Wiley & Sons, Ltd.

KEY WORDS erosion; overland flow; sediment yield; process-based model; numerical simulations

Received 4 February 2009; Accepted 8 January 2010

INTRODUCTION

The predictive capacities of process-based soil erosion models have been questioned in the literature (Favis-Mortlock, 1995; Jetten *et al*., 1999, 2003; Nearing *et al*., 2005). The main conclusions of these studies are that calibration is imperative for both field-scale and catchment scale models and that runoff is always better simulated than soil loss. Parsons *et al*. (2006) and Wainwright *et al*. (2008a) emphasize that the results of existing approaches remain incompatible with rates of long-term landscape evolution and with estimations over large spatial scales. They attribute this weak predictive capability to a fundamental misconception of the component processes that make up soil erosion. Wainwright *et al*. (2008a) criticize the assumption underlying many process-based erosion models that all movement occurs in suspension and question the flow detachment component proposed by Foster and Meyer (1972). Alternatively, Wainwright *et al*. (2008a) suggest an approach based on a transport distance concept; and Hairsine and Rose (1992) propose a continuous deposition approach recently implemented in a numerical model by Heng *et al*. (2009). Sander *et al*. (2007), Wainwright *et al*. (2008a) and Hairsine and Sander (2009) argue that the use of a transport capacity approach is not appropriate in the case of sediment transport on hill slopes. The debate about whether transport capacity, continuous deposition or transport distance is the best approach is not closed. There is probably no single approach valid for the whole range of particle size and density and the whole range of flow conditions on hill slopes (Nord *et al*., 2009). Spatiotemporal observations at high resolution of the hydraulics, erosion and morphology of the soil surface are needed to advance this subject.

An additional explanation for the weak predictive capability of process-based erosion models might be the limited understanding of the interaction between internal processes of overland flow and erosion at the local scale and the determination of dominant processes as a function of soil length and changing environmental conditions. The development of the Plot Soil Erosion Model_2D (PSEM_2D), which is a fully coupled physically based process model (infiltration-runoff-erosion), was an attempt to address this issue. The first version of the model was presented by Nord and Esteves (2005). Soil cohesion and the formation of a covering cohesionless layer as a result of sediment deposition and action of

* Correspondence to: Guillaume Nord, Institute of Environmental Assessment and Water Research, CSIC, Solé i Sabarís s/n, 08028 Barcelona, Spain. E-mail: guillaume.nord@idaea.csic.es

rainfall impact before runoff are represented explicitly. The erosion processes represented are rainfall and overland flow detachment of original soil, rainfall redetachment, overland flow entrainment of sediment from the covering cohesionless layer and deposition. This model allows modelling of Hortonian overland flow, infiltration and erosion during complex rainfall events over an irregular microtopography. The model also includes feedback between erosion and surface topography. Esteves *et al*. (2000) and Nord and Esteves (2005) gave the explicit finite difference schemes for coupling and solving the various equations. PSEM_2D was designed for applications at the plot scale (typically 100 m^2), with cell size characteristically $0{\cdot}25 \times 0{\cdot}25$ m. The application of the submodels for erosion processes at this spatial resolution is particularly appropriate, as it corresponds to the scale at which these submodels were developed and fitted with experimental dataset and thus have the greatest physical meaning (Knapen *et al*., 2007b; Gumiere *et al*., 2009).

The performance of the hydrological component of the model was tested by Esteves *et al*. (2000) by comparing the simulated discharges with hydrographs measured at the outlet of a 14·25-m long by 5-m wide plot based on the calibration of the infiltration parameters and the friction factor. The hydrology and hydraulics estimates were evaluated by Tatard *et al*. (2008) and compared with the results of MAHLERAN (Wainwright *et al*., 2008a) and Rillgrow2 (Favis-Mortlock *et al*., 2000). The comparison of simulated and observed flow velocity field measured over a 10×4 m experimental plot with a 1% slope showed that PSEM_2D was the most satisfactory model, at the cost of longer computational time. Nord and Esteves (2005) tested the first version of the erosion model on plane soil surfaces of $3 \times 0{\cdot}55$ m and $4{\cdot}58 \times 1{\cdot}52$ m against observed data and analytical results on the basis of calibrated hydrological and erosion parameters and completed a sensitivity analysis of the model parameters using the linear method. Nord and Esteves (2005) found that the dominant erosion process in these conditions was runoff detachment. Nord and Esteves (2007) evaluated an improved version of the erosion model that enables the comparison of four transport capacity formulae. The performance of the detachment-transport coupling model for erosion by runoff and four transport capacity formulae was tested in rill eroding conditions for five different textured soils without calibration of the erosion parameters, using the data collected by Elliot *et al*. (1989) in rills 9 m long by 0·5 m wide. The infiltration parameters were calibrated using flow discharge measurements; and the friction factor, using independent measurements of velocity. This constraining evaluation of the model showed that the Govers Unit Stream Power formula (Govers, 1992) gave the best results for cohesive soils. However, none of the equations performed well for non-cohesive soils.

Various studies (Sander *et al*., 2007; Wainwright *et al*., 2008a; Hairsine and Sander, 2009) criticize the use of the detachment-transport coupling model for entrainment and detachment by overland flow and deposition, as it is a discontinuous model, it was initially defined for steady-state conditions and it is based on the assumption that a specific flow possesses a specific capacity to transport sediment. We recognize part of these arguments, but we respond that there have been very few studies to apply this submodel at a scale that is really appropriate to evaluation. Nord and Esteves (2007) carried out such an evaluation and showed that the submodel gave acceptable spatial patterns of erosion and sediment loads for cohesive soils and was flawed for non-cohesive soils, but it was not clear whether this was because of numerical instabilities or inappropriate physical concepts. Recently, Heng *et al*. (2009) commented that the numerical problems associated with solving the Saint-Venant equations with varying topography are well known and that spurious waves can arise because of an imbalance between the flux gradient and the source terms in the momentum equation. Regarding the use of a transport capacity approach, Nord and Esteves (2007) and Nord *et al*. (2009) investigated the applicability of various transport capacity formulae for different conditions of size and density of particles and different modes of transport (suspension and bed load). Nord *et al*. (2009) observed that bed load transport capacity is independent of the suspended load transported by the flow and concluded that it was preferable to use different transport capacity equations and assumptions for each mode of transport. Therefore, we agree with the idea that model formalisms that are based on an overall transport capacity approach may be in error.

A complete evaluation of the PSEM_2D model at the plot scale would require a broad dataset, including measurements of soil moisture, soil properties, flow velocity field, flow discharge and sediment concentration at various locations, sediment properties and sediment tracing, which is not available at the moment. Wainwright *et al*. (2008c) recognize that there are significant difficulties in obtaining the spatial patterns of runoff and erosion data, which makes the evaluation of such models difficult. Recent applications of sediment tracing in the laboratory or in the field (Song *et al*., 2003; Polyakov and Nearing, 2004; Polyakov *et al*., 2004; Michaelides *et al*., 2010) offer an interesting perspective for determining the spatial patterns of erosion, but these articles generally disregard the spatial patterns of flow hydraulics and are therefore not directly comparable with modelling results.

This study proposed to carry out numerical simulation experiments of water erosion at the local scale (20 m long by 5 m wide) on an irregular surface, using PSEM_2D in a range of conditions for which the model had been fully tested beforehand. The conditions are limited to the case of cohesive soils in which suspended sediment is dominant. The limitations of the model, such as the use of a single particle size class, the absence of specific evaluation of the submodel for rainfall erosion, the absence of explicit representation of sediment transport by splash or raindrop-induced flow and disaggregation process, are recognized and taken into account in the Section on Discussion. The first objective is to test the effect of changing environmental factors (soil type,

meteorological forcing and slope gradient) on infiltration, runoff and sediment yield simulated by PSEM_2D at the outlet of a 20 × 5 m surface. The second objective is to analyse the changes in internal erosion processes simulated by PSEM_2D in response to the changes in these environmental factors. The third objective is to test the effect of microrelief, compared to a plane surface, on the internal erosion processes simulated by PSEM_2D. The final objective is to discuss the implications of the equations, concepts and parameterizations employed by PSEM_2D for the results given in this study.

MATERIAL AND METHODS

Description of the model

A detailed presentation of PSEM_2D was given by Esteves *et al*. (2000) and Nord and Esteves (2005). Infiltration is computed using a Green and Ampt model; overland flow is computed using depth-averaged two-dimensional unsteady flow equations (Saint-Venant equations); and soil erosion is computed by combining the equation of mass conservation of suspended sediment and a detachment-transport coupling model for erosion by runoff. Soil surface roughness is represented by the Darcy–Weisbach friction factor.

The structure of the erosion model is briefly described here. The mathematical basis for modelling of non-equilibrium sediment transport requires a mass balance equation for suspended sediment (Bennett, 1974):

$$\frac{\partial(hc)}{\partial t} + \frac{\partial(uhc)}{\partial x} + \frac{\partial(vhc)}{\partial y} = \frac{(D_{rd\_d} + D_{rd\_rd} + D_{fd\_d} + D_{fd\_e})}{\rho_s} \quad (1)$$

and a mass conservation for the deposited layer of loose sediment l_d, expressed in its most general form as:

$$\frac{\partial l_d}{\partial t} = -\frac{1}{\rho_s}(D_{rd\_rd} + D_{fd\_e}) \quad (2)$$

where h is the mean depth of flow, u and v the local depth-averaged velocities in the x- and y-directions, c is the volumetric sediment concentration, ρ_s the sediment particle density, D_{rd_d} the detachment rate of sediment by rainfall from original soil, D_{rd_rd} the redetachment rate of sediment by rainfall from the deposited layer, D_{fd_d} the detachment/deposition rate of sediment from original soil by overland flow and D_{fd_e} the entrainment/deposition rate of sediment from the deposited layer by overland flow.

Eroded sediment is transported as suspension only under the assumptions that the velocity of sediment is the same as flow velocity and that sediment concentrations are small enough so as not to appreciably influence the mechanisms of runoff (Bennett, 1974). The erosion processes and the detachment conditions are shown in Figure 1. First, at times or in locations where the shear stress of the flow is lower than the critical shear stress of the particle ($\tau < \tau_c$), the model does not represent explicitly the processes of raindrop detachment–splash transport (RD–ST) in the absence of runoff and of raindrop detachment–raindrop-induced flow transport (RD–RIFT) (Kinnell, 2005). As an alternative, we assume that bed elevation does not change during this phase and that the sediment concentration in flow remains zero, but that breakdown of aggregates, raindrop impact, rain splash and subsequent deposition contribute to filling up the buffer layer l_d:

$$\frac{\partial l_d}{\partial t} = \frac{1}{\rho_s}(D_{rd}) \quad (3)$$

where D_{rd} is the rate of aggregate breakdown and rainfall redistribution of sediment by splash and is expressed as:

$$D_{rd} = \alpha R\left(1 - \frac{h + l_d}{z_m}\right) \quad (4)$$

where R is the rainfall intensity, z_m the maximum penetration depth of raindrop splash and α the rainfall erodibility for original soil.

Secondly, at times or in locations where the shear stress of the flow overcomes the critical shear stress of the particle ($\tau > \tau_c$), the flow has a transport capacity and is able to entrain sediment from the layer of loose sediment. This phase, referred to as raindrop detachment–flow transport (RD–FT) by Kinnell (2005), explains an initial

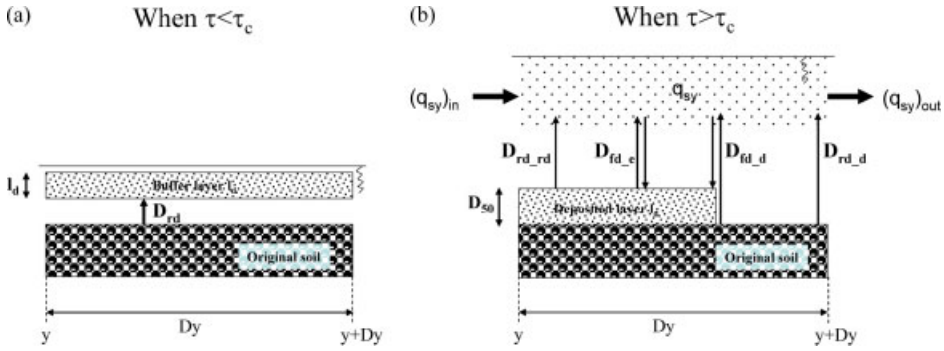

Figure 1. Erosion processes when the flow shear stress is (a) below the critical shear stress of the particle and (b) above the critical shear stress of the particle. D_{rd} is the rate of disaggregation and redistribution of sediment by rain splash, D_{rd_d} the sediment detachment rate from original soil by rainfall, D_{rd_rd} the sediment redetachment rate from the deposited layer by rainfall, D_{fd_d} the detachment/deposition rate of sediment from original soil by runoff and D_{fd_e} the entrainment/deposition rate of sediment from the deposited layer by runoff

peak of sediment concentration due to the flushing of the layer of loose sediment. The variable defined as $\varepsilon = \frac{l_d}{D_{50}}$ enables us to differentiate between the rainfall detachment and rainfall redetachment rates at the sub-grid scale:

Detachment:

$$D_{rd\_d} = \alpha R \left(1 - \frac{h}{z_m}\right)(1 - \varepsilon) \tag{5}$$

Redetachment:

$$D_{rd\_rd} = \alpha_d R \left(1 - \frac{h}{z_m}\right)\varepsilon \tag{6}$$

where α_d is the rainfall erodibility for the layer of loose sediment.

The conceptualization of the model implies that the transport of sediment by rainfall-driven erosion processes (which occur when $\tau < \tau_c$) is delayed and controlled by the energy of overland flow. In the current version of the model, as transport by rain splash is not explicitly represented, we recognized that it is a limitation of the model that makes it inappropriate to applications at the very local scale ($\sim$1 m^2). Once the flow shear stress is higher than the critical shear stress of the soil τ_{soil}, runoff detachment of original soil is initiated. This situation is referred to as flow detachment–flow transport (FD–FT) by Kinnell (2005). Entrainment and detachment by overland flow and deposition are ruled by the detachment-transport coupling model proposed by Foster *et al*. (1995). Net erosion takes place when sediment discharge is less than sediment transport capacity:

Detachment:

$$D_{fd\_d} = K_r(\tau - \tau_{soil})\left(1 - \frac{q_s}{T_c}\right)(1 - \varepsilon) \tag{7}$$

Entrainment:

$$D_{fd\_e} = K_r(\tau - \tau_c)\left(1 - \frac{q_s}{T_c}\right)\varepsilon \tag{8}$$

where K_r is the flow erodibility parameter, τ_{soil} the critical shear stress of original soil, q_s the sediment discharge per unit flow width in the flow direction and T_c the sediment transport capacity formula.

Net deposition occurs when sediment discharge is higher than sediment transport capacity:

$$D_{fd\_d} + D_{fd\_e} = \frac{\varphi V_f}{q}(T_c - q_s) \tag{9}$$

where φ is a raindrop-induced turbulence coefficient, V_f the particle settling velocity and q the flow discharge per unit width in the flow direction.

In this study, we decided to work with cohesive soils for which suspended sediment transport is dominant and we selected the Govers Unit Stream Power formula (Govers, 1992) that gave the best results for such conditions (see Nord and Esteves, 2007):

$$T_c = \frac{86{\cdot}7(S_f\overline{V} - 0{\cdot}005)}{\sqrt{D_{50}}}q \tag{10}$$

where S_f is the energy slope and $\overline{V}$ is the depth-averaged flow velocity in the flow direction.

Numerical experiment

The simulated area was 20 m long and 5 m wide (100 m^2). Several environmental factors, including slope, meteorological forcing and soil properties, were tested.

Topography. The digital elevation model (DEM) used in this study was originally derived from a plot in Niger surveyed by Esteves *et al*. (2000) on 0·25 m

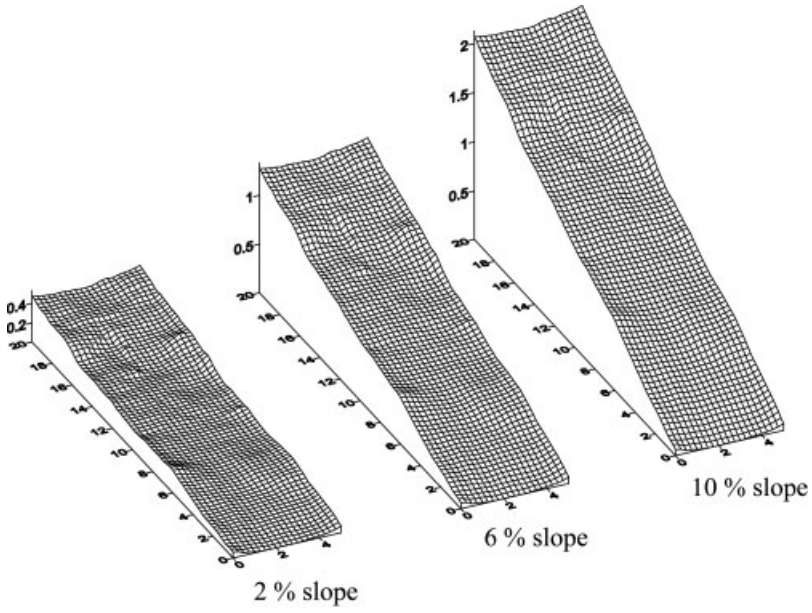

Figure 2. Simulated areas of 20 × 5 m employed in the numerical experiment. Mean longitudinal slope gradients are respectively 2, 6 and 10%. The microrelief is the same in the three cases. Measurements are in meters

grids. This plot had a mean longitudinal slope of 5·1%. The microrelief was extracted by subtraction between the DEM of the natural surface and the DEM of a plane surface with a longitudinal slope of 5·1%. A correction was applied to account for the projection of the microrelief on a horizontal plane. The microrelief was lightly modified at the base slope to enhance the concentration of overland flow into a main rill. The choice of an observed microrelief was preferred to a statistically generated one to allow simulation of a realistic hydrographic network. The coefficient of random roughness of the microrelief, defined as the standard deviation of the measured height at regular intervals, was 0·032 m. The minimum height was −0·036 m, the maximum height was 0·142 m and the averaged height was 0·037 m. The microrelief was then projected on three surfaces of 20 × 5 m with mean longitudinal slopes of 2, 6 and 10% to be tested in this numerical experiment, as illustrated in Figure 2. The mean longitudinal slope gradients were selected as being within the range of slopes currently studied in erosion experiments, where inter-rill and rill erosion are commonly observed (Govers and Poesen, 1988; Elliot *et al*., 1989; Parsons *et al*., 1991; Brunton and Bryan, 2000; Chaplot and Le Bissonnais, 2000; Planchon *et al*., 2005; Cerdan *et al*., 2006).

It is questionable to use the same microrelief with different environmental settings, inasmuch as other feedbacks such as climate, geology and vegetation are expected to control the way the soils, slope surface and microtopography develop. However, these feedbacks are not supposed to be significant at the time scale of the storm event. Furthermore, this study does not aim to reproduce observed results, but rather to estimate the sensitivity of the model to changes in environmental conditions and to discuss the validity of the equations, concepts and parameterizations based on spatially distributed results.

Meteorological forcing. The rainfall hyetographs of the four events selected in this study are shown in Figure 3 and the main descriptive statistics are given in Table I. The two storms of the temperate climate (storm 1 and storm 2) were selected from the Ganspoel dataset (Van Oost *et al*., 2005) and were also previously chosen by Nearing *et al*. (2005), who investigated the response of seven soil erosion models to a few basic precipitation- and vegetation-related parameters. The data were available at 1-min resolution. Storm 1 was a short thunderstorm with a significant amount of rainfall typical of the summer period. Storm 2 was a long rainfall event with a major amount of rainfall and a low rainfall intensity associated with an oceanic front. Storm 3 was measured in Nîmes (France) and was seen as a major Mediterranean summer thunderstorm. The data were available at 5-min resolution. The event had a relatively short duration but a high rainfall amount and very high rainfall intensities. The event consisted of a first strong rain shower followed by longer and less intense rain (Figure 3). It was decided to invert the rainfall hyetographs of this event to produce the reversed 12 September 2004 storm (storm 4) and so test the effect of the delayed occurrence of a strong rain shower on the production of runoff and erosion. In terms of recurrence period, these events were all classified as extreme events, since their recurrence periods, calculated on the basis of the intensity-duration-frequency curves

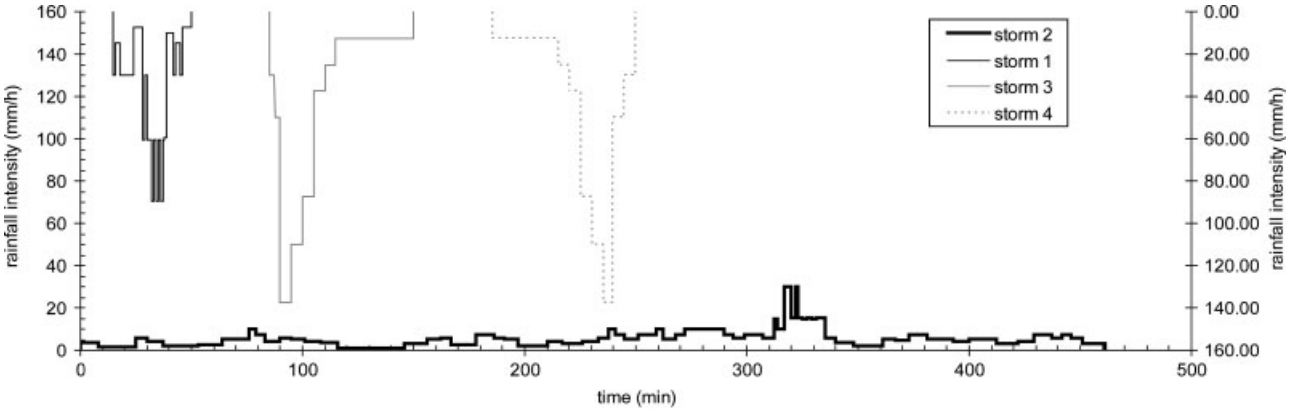

Figure 3. Hyetograms of the four rainfall events used in the numerical experiments

Table I. Descriptive statistics of the rainfall events

Storm number	Location	Climate	Date	Precipitation amount (mm)	Mean rainfall intensity (mm/h)	Maximum 5-min rainfall intensity (mm/h)	Maximum 30-min rainfall intensity (mm/h)	Duration (min)
1	Ganspoel (Belgium)	Temperate	11 July 1997	19·5	33·4	77·7	35·8	35
2	Ganspoel (Belgium)	Temperate	14 September 1998	41	5·3	24·0	13·6	460
3	Nîmes (France)	Mediterranean	12 September 2004	44	40·6	137·5	72·9	65

of each region, were in the range of 5–10 years. These observed events representative of two distinct climates were selected to test the applicability of the equations used in the model under non-steady conditions and to evaluate the sensitivity of the model to different structures of rainstorms.

Soil properties. Three different cohesive soils were chosen for this numerical experiment: clay loam, silty clay loam and silt loam. These soils are common among cultivated soils. They represent a wide range of soil types and their erodibility has been widely tested in the laboratory, in the field and numerically (Elliot *et al*., 1989; Nearing *et al*., 1997; Chaplot and Le Bissonnais, 2000; Hairsine *et al*., 2002; Leguédois and Le Bissonnais, 2004; Nord and Esteves, 2007). The approach followed in this study was to propose a combination of realistic parameters for each type of soil based on various studies of infiltration, detachment and redetachment by rainfall impact, detachment by runoff and sediment size and density. The sets of parameters for each textured soil are given in Table II. The parameters for infiltration (K_s, $\theta_s - \theta_i$ and h_f) were selected on the basis of the results of Rawls *et al*. (1983), Elliot *et al*. (1989) and Nord and Esteves (2007). The parameter for detachment by rainfall impact (α) was selected on the basis of the findings of Leguédois (2003) and Leguédois and Le Bissonnais (2004). The parameter for redetachment by rainfall impact (α_d) was set one order of magnitude greater than α, following the observations of Proffitt *et al*. (1991), although there are very few references on this question in the literature. Heng *et al*. (2009) calibrated the detachability parameter of undisturbed soil and the detachability parameter of deposited sediment and found that the second parameter was 15 times greater than the first one. The parameter for detachment by runoff (K_r and τ_{soil}) and sediment properties (D_{50} and ρ_s) were selected on the basis of the results of Elliot *et al*. (1989), Foster *et al*. (1995) and Nord and Esteves (2007). The values of D_{50} and ρ_s, were influenced by the property of the soil type to producing aggregates among eroded soil fragments. D_{50} is lower than 100 μm for the three soils, which ensures that suspension is dominant. The erodibility parameters were assumed static in this study, as we worked on the time scale of the storm event. Knapen *et al*. (2007a) demonstrated the need to take into account the intra-seasonal variations in K_r and τ_{soil}, but it is more critical to apply this in the case of continuous erosion modelling.

Parameterization of frictional resistance of overland flow. So far, except in a very limited number of cases like Walnut Gulch (Scoging *et al*., 1992; Abrahams *et al*., 1995, 1996), the predetermination of the value of the friction factor is not feasible, because of the lack of distributed data of flow velocity. Very little progress will be made in this area until more research is undertaken to make the necessary measurements. In this study, we followed an approach similar to that described by Hairsine and Sander (2009) for fitting the friction factor. Some studies have shown that the friction factor depends on the inundation ratio and varies with hydraulic conditions (Gilley *et al*., 1992; Lawrence, 1997). Nearing *et al*. (1997) demonstrated that predictive relationships for estimating the friction factor could not be used unless abundant soil information was obtained. Nord and Esteves (2007) calibrated the friction factor in eroding rills for different values of water discharge and for different textured soils and reported that the friction factor varied for each soil type. A numerical experiment by Tatard *et al*. (2008) using PSEM_2D and distributed data of flow velocity demonstrated that the friction factor should be lower in rill than in inter-rill. Based on these results and the studies by Esteves *et al*. (2000) and Nord and Esteves (2005), we assumed that it was more important to take into account the distinction between rill and inter-rill in terms of friction factor parameterization than the distinction between soil types. A constant value of 0·4 was applied for the friction factor over the entire simulated area, excluding the main rill located at the bottom of the plot, where a value of 0·2 was set. The same values were used for the three soil types. Such values are consistent at the grid resolution employed in this study (cell size of 0·25 × 0·25 m), but would not make sense at a coarser grid resolution. Wainwright *et al*. (2008c) demonstrated that the value of the friction factor is dependent on the grid resolution.

Table II. Parameterization of infiltration, soil erodibility and sediment properties in PSEM_2D for the different soil textures

Parameters	Dimension	Clay loam	Silt loam	Silty clay loam
Infiltration				
K_s	m/s	4.10–7	8.10–7	2.10–7
$\theta_s - \theta_i$	—	0·2	0·2	0·2
h_f	m	0·2	0·3	0·6
Soil erodibility				
α	kg/m^2/ mm	0·008	0·015	0·010
α_d	kg/m^2/ mm	0·08	0·15	0·10
K_r	s/m	0·005	0·020	0·010
τ_{soil}	Pa	2·5	6·0	5·0
Sediment properties				
D_{50}	mm	100	50	20
ρ_s	kg/m^3	2000	2000	2000

Data analysis

Combining all the environmental factors, 36 simulations were run (3 slopes × 4 storms × 3 soils). Results were analysed at the outlet of the 100 m^2 simulated area (20 m long by 5 m wide) and at different positions along the main slope length (4, 8, 12, 16 and 20 m).

Numerical tracing of sediment

The simulated area of 100 m^2 was divided into five subplots of 20 m^2 (4 m long by 5 m wide). Soil from each subplot was tagged in a different way, i.e. a number from 1 to 5 was assigned to each subplot. Source terms

Table III. Results of the simulations at the outlet of the simulated area

Storm	Soil	Slope (%)	Infiltration volume (l)	Runoff volume (l)	Runoff coefficient (%)	Flood duration (s)	Flow discharge		Flow shear stress			Sediment concentration		Sediment discharge		Sediment yield (kg)	Deposit (kg)	Detachment rainfall (kg)	Redetachment rainfall (kg)	Detachment flow (kg)	Entrainment flow (kg)
							Peak (l/min)	Mean (l/min)	Max (Pa)	Median (Pa)	$\tau > \tau_{soil}$[a] (%)	Max (g/l)	Mean (g/l)	Max (kg/s)	Mean (kg/s)						
1	CL	2	828	1133	60·5	2070	120·6	32·4	3·3	0·2	0·8	1·2	0·4	0·002	0·001	0·9	17·3	3·0	14·2	0·5	0·3
		6	812	1158	61·0	1831	123·7	37·4	5·1	0·4	2·8	11·6	4·6	0·023	0·006	9·4	17·6	6·5	13·6	6·1	1·6
		10	811	1151	60·6	1711	128·1	39·1	6·4	0·7	6·6	23·2	13·5	0·048	0·013	21·2	4·6	9·1	5·0	11·0	1·8
	SL	2	1229	708	37·8	1350	96·3	30·8	2·8	0·1	0	4·6	1·1	0·004	0·001	1·2	64·0	2·2	63·5	0·0	0·3
		6	1210	735	38·7	1260	100·0	34·1	4·1	0·3	0	34·3	7·6	0·018	0·005	5·9	66·4	7·4	64·4	0·0	2·0
		10	1210	730	38·4	1201	103·3	35·5	4·7	0·5	0	82·9	26·3	0·044	0·013	16·7	33·3	12·9	34·6	0·0	3·5
	SCL	2	937	1019	54·4	1740	116·0	34·0	3·2	0·2	0	9·3	3·8	0·064	0·004	6·8	51·8	3·4	44·8	0·0	0·5
		6	921	1041	54·8	1530	118·5	39·3	4·7	0·4	0·0	27·9	7·1	0·021	0·006	8·7	37·9	7·2	39·3	0·0	1·1
		10	921	1035	54·5	1501	121·9	39·8	5·8	0·7	0·5	106·0	18·8	0·034	0·010	14·4	14·8	10·9	16·7	0·5	1·7
2	CL	2	2935	1174	29·4	14734	38·5	4·8	1·7	0·1	0	2·9	0·0	0·002	0·000	0·2	17·6	0·6	16·9	0·0	0·4
		6	2920	1199	29·6	13868	45·8	5·2	2·3	0·2	0	16·4	1·6	0·005	0·000	2·4	28·5	2·6	26·4	0·0	2·9
		10	2920	1197	29·6	13689	46·0	5·2	1·9	0·2	0	35·0	6·3	0·017	0·001	10·4	22·5	6·1	21·7	0·2	7·1
	SL	2	3804	263	6·5	1980	23·7	7·8	1·3	0·0	0	3·6	0·8	0·001	0·000	0·3	22·8	0·1	22·7	0·0	0·5
		6	3775	292	7·2	1681	36·1	10·2	1·5	0·1	0	53·9	11·4	0·019	0·002	3·4	40·9	0·9	39·7	0·0	4·6
		10	3775	291	7·2	1621	35·6	10·6	1·5	0·1	0	118·0	34·7	0·054	0·007	11·4	43·7	2·3	44·2	0·0	9·7
	SCL	2	3080	1025	25·7	13353	37·0	4·6	1·7	0·1	0	6·2	0·8	0·003	0·000	1·5	65·9	0·9	53·6	0·0	0·5
		6	3068	1043	25·7	12488	45·1	5·0	2·2	0·2	0	48·0	3·1	0·012	0·000	4·8	98·7	2·5	99·9	0·0	3·6
		10	3068	1041	25·7	12309	44·6	5·0	2·6	0·3	0	107·6	10·8	0·028	0·001	15·6	84·6	8·0	82·7	0·0	11·6
3	CL	2	1236	3387	77·8	4261	215·1	47·4	4·4	0·3	1·9	2·3	0·5	0·008	0·001	5·0	58·7	8·5	51·6	4·2	0·3
		6	1218	3367	77·0	3961	215·2	50·6	7·2	0·7	6·2	15·3	4·3	0·052	0·010	36·8	42·9	18·0	33·7	29·1	0·9
		10	1218	3343	76·4	3931	213·5	50·7	9·1	1·0	18·2	34·7	11·2	0·122	0·021	82·4	7·5	24·9	6·2	59·9	1·0
	SL	2	2083	2471	56·7	3721	187·0	39·5	4·1	0·2	0	4·6	1·0	0·008	0·002	4·9	151·1	11·8	147·0	0·0	0·3
		6	2063	2465	56·3	2762	187·1	52·5	6·2	0·6	0·2	39·0	6·8	0·044	0·008	18·7	115·6	26·6	109·1	0·0	1·4
		10	2062	2451	56·0	2642	186·5	54·4	7·8	1·0	0·9	62·9	22·1	0·090	0·020	46·1	29·7	39·5	30·9	5·2	1·8
	SCL	2	1425	3189	73·2	4201	209·1	45·2	4·3	0·3	0	8·9	1·8	0·016	0·002	9·0	79·1	15·0	72·3	0·0	0·1
		6	1409	3162	72·3	3901	208·4	48·3	6·6	0·7	0·9	19·4	4·5	0·044	0·007	25·3	73·1	23·8	73·0	3·6	0·5
		10	1409	3144	71·9	3841	207·6	48·8	8·8	1·0	2·1	58·9	11·0	0·070	0·013	48·0	32·2	31·8	31·3	16·7	1·3
4	CL	2	1132	3739	81·6	2971	234·2	74·8	4·2	0·2	1·4	2·7	1·1	0·010	0·003	6·3	80·2	7·1	74·7	5·2	0·6
		6	1112	3731	81·0	2611	232·2	84·8	8·7	0·7	5·9	15·6	8·4	0·060	0·020	43·9	56·0	17·4	48·0	34·3	2·8
		10	1111	3702	80·4	2581	231·1	85·1	11·5	1·0	19·1	36·5	19·9	0·139	0·042	98·8	10·3	24·7	11·8	72·1	3·0
	SL	2	1723	3110	67·8	2251	220·4	81·8	4·4	0·3	0	7·5	1·9	0·010	0·004	6·6	194·9	9·6	195·3	0·0	0·6
		6	1692	3109	67·5	2040	217·6	90·1	6·7	0·7	0·6	40·3	8·0	0·032	0·013	25·0	154·1	26·7	151·3	1·0	3·9
		10	1691	3088	67·1	2011	216·8	90·8	9·2	1·1	1·4	91·8	22·5	0·083	0·032	62·2	51·2	41·8	56·1	11·4	5·9
	SCL	2	1256	3609	78·7	2640	231·5	81·1	4·5	0·3	0	6·3	3·2	0·018	0·006	12·3	94·5	13·6	93·1	0·0	1·0
		6	1233	3597	78·1	2311	229·1	92·2	7·3	0·7	1·5	33·8	8·1	0·040	0·014	31·3	68·1	23·4	71·7	5·3	1·6
		10	1232	3569	77·5	2250	227·9	93·9	10·7	1·1	2·2	85·3	17·5	0·078	0·025	56·8	22·8	31·2	25·9	20·4	3·0

[a] $\tau > \tau_{soil}$ (%) means the percentage of the plot surface that has a flow shear stress higher than the critical shear stress of original soil.
CL, clay loam; SL, silt loam; SCL, silty clay loam.

for erosion processes were also tagged accordingly and Equation 1 was solved five times at every time step, using the same scheme as that described by Nord and Esteves (2005), over the whole simulated area to calculate five sediment concentrations and calculate the contribution from each subplot to the sediment yield at the outlet of the 100 m^2 simulated area. The total sediment concentration was calculated as the sum of these five concentrations. These developments were incorporated in another version of the model and simulations were run again with this latter version (36 runs in total). The results simulated by the two versions of the model were compared. Differences between the results appeared in a few cases. It was found that the schemes used for coupling the Saint-Venant equation and the five equations of mass conservation of suspended sediment caused local crashes in the calculation of flow velocity and sediment concentration for three simulations on the 2% slope. Furthermore, the process of flow detachment was enhanced for 11 simulations due to numerical instabilities in the main rill near the slope base. These 14 simulations were removed and a total of 22 simulations were selected for the analysis.

RESULTS AND DISCUSSION

Effects of environmental factors on the simulated results of PSEM_2D at the outlet of the 20 × 5 m surface area

The main results of the simulations at the outlet of the simulated area are shown in Table III. The largest runoff volumes are simulated for storm 4, followed by storms 3, 1 and 2. In the case of storms 3 and 4, it should be noted that the reversed rainfall hyetograph gives significantly more runoff (up to 30%) than the normal rainfall hyetograph does. The period of low rainfall intensity that takes place at the beginning of the event causes progressive saturation of the soil, which enhances runoff during the final rain shower. Flow discharge is minimum for storm 2 and maximum for storm 4. The fact that rainfall intensity is the variable that controls the magnitude of the runoff response is explained by the selection of the Green and Ampt model, which only simulates Hortonian overland flow generation. In terms of soil type, clay loam gives the largest runoff volumes, followed by silty clay loam and silt loam. These results are directly related to the values of the infiltration parameters (K_s, h_f) selected in this study.

Storm 4 produces the highest values of sediment yield, followed by storms 3, 1 and 2. These results corroborate the results obtained for runoff volumes. However, sediment yield ranges over more than two orders of magnitude (from 0·2 to 98·8 kg), whereas runoff volume ranges over only one order of magnitude (from 263 to 3739 l) when all the simulations are considered. A deeper look at the results shows that an increase in runoff volume does not always coincide with an increase in sediment yield and inversely. These results support the use of a fully coupled model (infiltration-runoff-erosion) to understand the dominant processes at the 100 m^2 scale and the interactions between all the processes within the simulated area.

Figure 4 shows the results of sediment yield (soil loss per unit area) versus runoff coefficient for the 100 m^2 simulated area. The same results are plotted in three different ways to assess the effect of environmental factors on runoff coefficient and sediment yield. Results are grouped by soil texture in Figure 4(a), storm event in Figure 4(b) and slope gradient in Figure 4(c). There is an overall positive relationship between runoff coefficient and sediment yield, as Parsons *et al*. (2006) observed, although in their case the relationship was much stronger. Maximum sediment yield reaches approximately 1 kg/m^2 and is simulated for the case of clay loam with storm 4 and 10% slope. This is a very high value of sediment yield, which is the consequence of the combination of extreme conditions: low infiltrability, a low value of the critical shear stress of original soil, a severe Mediterranean thunderstorm (period of recurrence in the range of 5–10 years) and a steep slope. Figure 4(a) shows that sediment yield is weakly sensitive to soil type in this study. It may be related to the use of the same friction factor parameters for the three soil types and the absence of feedback between flow hydraulics and friction parameter. Figure 4(b) shows how storms 3 and 4 produce the highest runoff coefficients and the highest sediment yields. Storms 3 and 4 have the greatest maximum 5-min rainfall intensity, attaining 137·5 mm/h as seen in Table I. In Equations (5) and (6), the rainfall detachment and redetachment rates are proportional to rainfall intensity; and in Equation (10), transport capacity is a function of flow

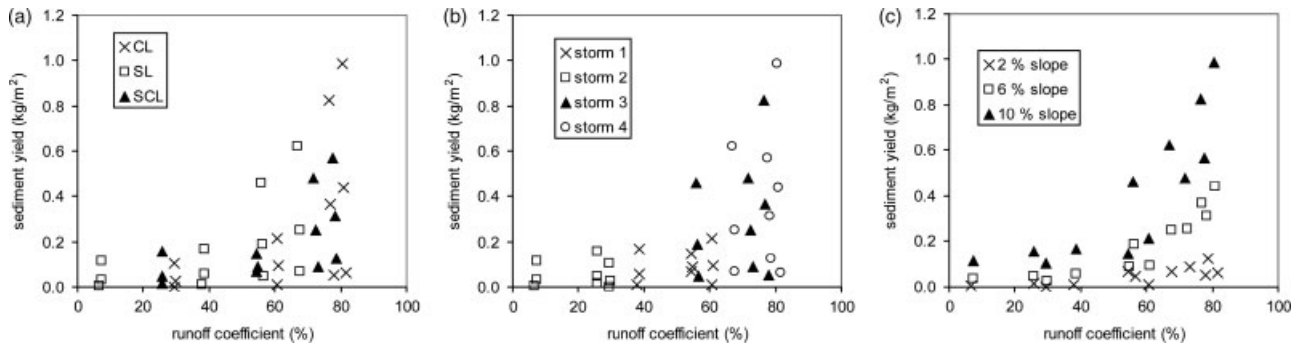

Figure 4. Sediment yield versus runoff coefficient for the 100 m^2 simulated area. Results are grouped by (a) soil texture; (b) storm event and (c) slope gradient

discharge. Storm 4 produces more runoff and more sediment yield than storm 3. The structure of storm 4, with the highest rainfall intensities at the end of the event, is more harmful in terms of soil loss than the structure of storm 3. Storm 2 produces the lowest runoff coefficient and sediment yield due to low rainfall intensities. Storm 1 gives a higher runoff coefficient than storm 2, but sediment yield is of the same order of magnitude. Figure 4(c) shows that runoff coefficient is not sensitive to slope gradient in this study. This result may be explained by the choice of homogeneous infiltration and friction factor parameters over the simulated area, the limited slope length of the simulated area (20 m) and the use of relatively coarse time steps for rainfall (1 or 5 min). These conditions may lead to the underestimation of the runoff response and the lack of reinfiltration during periods of low rainfall intensity (Wainwright and Parsons, 2002).

However, sediment yield is positively related to slope gradient. In Equation (10), transport capacity is a function of slope energy that depends on slope gradient; and in Equations (7) and (8), flow detachment and entrainment rates are functions of shear stress that also depends on slope gradient. In this study, the friction factor is constant over time and only accounts for grain roughness. Form roughness is not taken into account and friction factor is not a function of flow hydraulics. The experimental studies carried out by Giménez and Govers (2001) showed the slope independence of rill flow velocities on mobile beds where form roughness can develop due to a feedback between rill bed morphology and flow conditions. Giménez and Govers (2002) explained that form shear stress, which is dissipated on bed irregularities, does contribute to soil detachment, but does not contribute to sediment transport. The significant sensitivity of sediment yield to slope gradient in this study may be caused by the assumptions and choices made to represent and parameterize surface roughness.

Changes in internal erosion processes simulated by PSEM_2D in response to changes in environmental factors

The range of sediment yield versus slope length is plotted in Figure 5. All the simulations of Table III are taken into account. Five slope lengths are considered (4, 8, 12, 16 and 20 m). Sediment yield (in kg/m^2) decreases overall between 4 and 8 m before increasing further downstream and reaching its highest values at 20 m. Variability is important all over the plot and is greatest at 20 m. Seventy-five percent of the values of sediment yield are lower than 0·2 kg/m^2 for slope lengths ranging from 4 to 16 m and lower than 0·3 kg/m^2 for a slope length of 20 m, which corresponds to an increase of 50% between 16 and 20 m. The values of sediment yield simulated in this study are of the same order of magnitude as those given by Parsons *et al.* (2006) for plots with areas of 21·01, 115·94, 56·84 and 302·19 m^2 and lengths of 4·12, 14·48, 18·95 and 27·78 m under natural storm events.

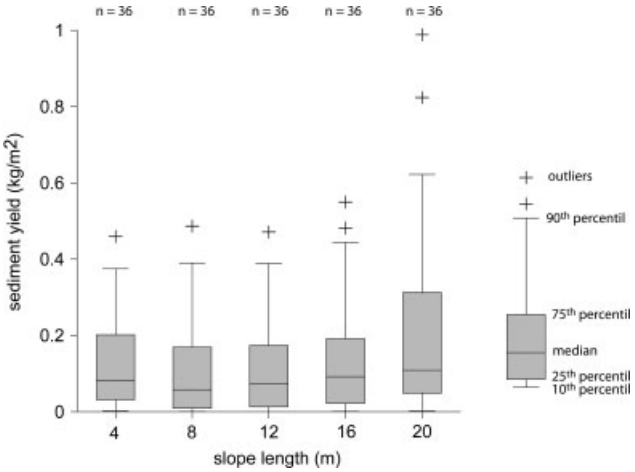

Figure 5. Range of sediment yield versus slope length

Figure 6 shows the range of the contribution of rainfall erosion processes to gross erosion versus slope length. Whereas rainfall erosion (in kg) is the sum of rainfall detachment and rainfall redetachment, flow erosion (in kg) is the sum of flow entrainment and flow detachment. Gross erosion (in kg) is the sum of rainfall detachment, rainfall redetachment, flow entrainment and flow detachment. The contribution of rainfall erosion processes to gross erosion is calculated as the fraction of rainfall erosion to gross erosion simulated over five surfaces of different slope lengths (4, 8, 12, 16 and 20 m) and constant width (5 m) that all have the same upstream border and whose areas range from 20 to 100 m^2. The median of the contribution of rainfall erosion processes to gross erosion varies between 97·5 and 98·2% for surfaces with slope lengths between 4 and 16 m and decreases to 93·2% for surfaces with a slope length of 20 m. The contribution of rainfall erosion to gross erosion is dominant for all surfaces with slope lengths ranging from 4 to 20 m. The contribution of rainfall erosion to gross erosion is particularly high and uniform in the upper part of the simulated area (for slope length lower or equal to 12 m) and decreases unevenly for surfaces with greater slope length. The change that appears for surfaces whose slope length is between 12 and 16 m is caused by the activation of flow detachment. High variability in the results, especially for surfaces with slope lengths of 16 and 20 m, is because activation of flow detachment is mainly controlled by hydraulic conditions and soil properties by means of Equation 7, which involves a threshold on shear stress ($\tau > \tau_{soil}$). Wainwright *et al.* (2008b) performed a sensitivity analysis of MAHLERAN on a uniform, planar 100-m long by 30-m wide slope and remarked that raindrop detachment was the dominant process of erosion for slope lengths ranging from 0 to 20 m. Concentrated erosion was activated between 20 and 100 m in function of the conditions of rainfall intensity, rainfall duration, slope angle, particle size and friction factor. The use of a planar surface explains that concentrated erosion was activated further downstream on the slope than in our results. In this study, the erosion

regime is generally limited by transport capacity up to 12 m. In this zone, rainfall erosion processes prevail, but flow transport capacity is low, due to the small contributive area and the weak degree of concentration of overland flow. Transport of sediment off-site is ruled by overland flow in PSEM_2D. Transport by splash or raindrop-induced flow is not represented in the model, which might underestimate sediment export, especially in the upper part of the simulated area. For slope lengths greater than 12 m, the erosion regime is either limited by detachment (if flow detachment remains absent) or not limited at all (if flow detachment is activated). Activation of flow detachment often appears between 12 and 16 m. A transport-limited regime on the lower part of the slope is not simulated in this study. It would take place further downstream if a larger area or a slope break was simulated.

Figure 7 gives the results of sediment yield (in kg/m^2) versus slope length for each environmental factor. The results that were plotted in Figure 5 are at present classified and averaged by soil type in Figure 7(a), storm event in Figure 7(b) and slope gradient in Figure 7(c). This way of plotting does not represent the variability of the results, but does enable the effect of each environmental factor on sediment yield along the main slope length of the simulated area to be assessed. Figure 8 applies the same approach for the contribution of rainfall erosion processes to gross erosion. All these results were simulated and do not necessarily represent the behaviour of erosion on actual soils. Certain processes such as soil crusting are not included in this study. Figure 7(a) shows that clay loam has lower sediment yield than silt loam and silty clay loam in the upper part of the simulated area (up to a slope length of 12 m) and that this order is reversed at the base of the slope. Figure 8(a) shows that rainfall erosion dominates for all surfaces, independently of slope length and soil texture. Clay loam is the only soil type for which flow erosion is really activated in the lower part of the simulated area. The start of flow detachment explains the rapid increase in sediment yield with slope length for clay loam after 12 m in Figure 7(a). At 4, 8 and 12 m, sediment yield correlates negatively with median particle sediment diameter, which illustrates a case of transport-limited regime. It means that the finer the particle diameter, the higher the sediment yield. However, at 20 m, sediment yield correlates negatively with shear stress of original soil (τ_{soil}), which illustrates a case of detachment-limited regime. In such conditions, the particle size becomes a secondary factor to explain sediment yield and the shear stress of original soil (τ_{soil}) becomes the dominant factor. The model uses a single representative class, whereas in reality there is a wide range of size classes. These results suggest that the representation of a wide range of size classes in the erosion models is more justified for the cases where slope length is lower than 12 m. For longer slopes, the accurate representation of the start of flow detachment might be more important. Studies such as that of Leonard and Richard (2004), which focused on the direct or indirect measurement of τ_{soil}, are therefore essential to the accurate prediction of erosion by means of process-based models.

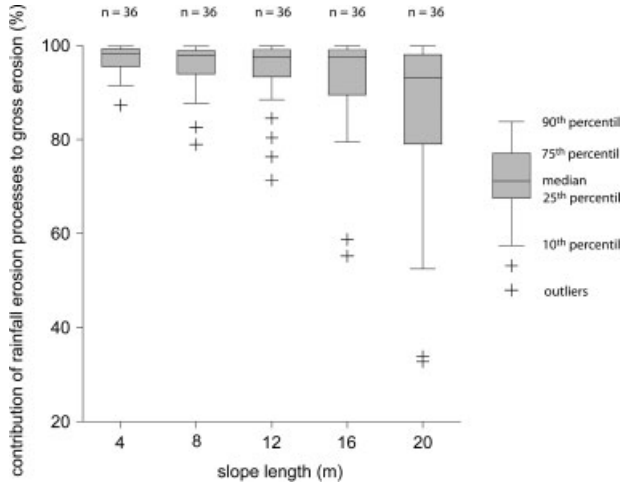

Figure 6. Range of contribution of rainfall erosion processes to gross erosion for surfaces of different slope length

As seen in Figure 7(b), storms 3 and 4 have average values of sediment yield 2·5–5 times greater than storms 1 and 2 at all the positions along the slope. Sediment yield does not vary significantly with slope length for storms 1 and 2. For storms 3 and 4, sediment yield is almost constant up to 12 m and increases rapidly with slope length downstream to reach average values of 0·3–0·4 kg/m^2 for slope length of 20 m. Figure 8(b) shows that rainfall erosion causes almost 100% of gross

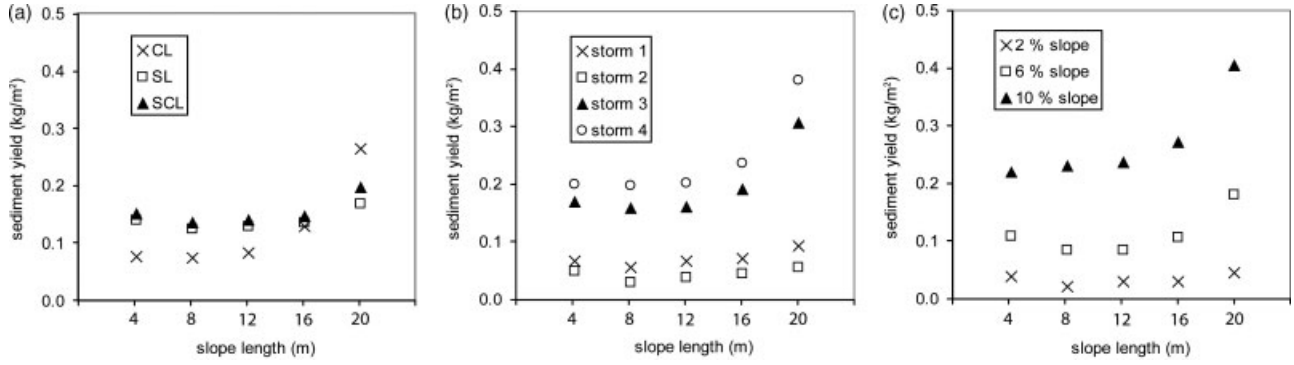

Figure 7. Sediment yield versus slope length. Results are grouped by (a) soil texture; (b) storm event and (c) slope gradient. Each point is the mean of 9 or 12 results

erosion for all surfaces, independently of slope length for storms 1 and 2. For storms 3 and 4, rainfall erosion still dominates largely for all surfaces, but flow erosion becomes significant between 16 and 20 m. The high runoff volumes and high flow discharges simulated for these storms 3 and 4, as seen in Table III, are responsible for activation of flow erosion and high sediment transport in the main rill located on the lower part of the slope, which explains the sudden rise of sediment yield with slope lengths between 16 and 20 m.

Figure 7(c) shows that, for the 2% slope, sediment yield remains constant all over the simulated area. For the 6% slope, sediment yield has a minimum at 12 m, an intermediate maximum at 4 m and a larger maximum at 20 m. For the 10% slope, sediment yield increases continuously with slope length. The highest rise takes place between 12 and 20 m and the average value of sediment yield reaches 0·4 kg/m^2 at 20 m. The results plotted in Figure 8(c) show that, for the 2% slope, rainfall erosion causes almost 100% of gross erosion for all surfaces, independently of slope length. For the 6 and 10% slopes, the contribution of rainfall erosion remains dominant on average for all surfaces, independently of slope length, but it decreases with slope length and slope gradient. The start of flow erosion takes place further upstream as the slope gradient increases. The highest sediment yields are simulated on the lower part of the slope and correspond to cases where flow erosion is well activated (lower contribution of rainfall erosion to gross erosion). Song *et al*. (2003) observed that, once rill erosion began, erosion amounts at the outlet of the plot increased severely and suddenly. The combination of high runoff volumes and strong slopes is responsible for high transport capacity and activation of flow erosion in this study. The lower value of the friction factor in the main rill located at the bottom of the simulated area also causes an acceleration of overland flow in this zone and increased transport capacity [Equation (10) is a function of flow velocity], which converts into an increase in the flow detachment rate by means of the detachment-transport coupling model [Equation (8)]. The presence of the main rill at the base of the slope is probably responsible for the rapid increase in sediment yield between 16 and 20 m in Figures 5 and 7.

Figure 9 shows the range of contribution of five slope segments of 20 m^2 to the total sediment yield at the outlet of the simulated area. Fourteen of the 36 simulations had excessive divergence, in comparison with the results obtained with the version of the model without numerical tracing, and were excluded from this analysis. The results of Figure 9 show that sediment exported at the outlet of the simulated area comes predominantly from the subplot located near the outlet. The two slope segments 8–12 and 12–16 m contribute less to the total sediment yield at the outlet; and the two slope segments 0–4 and 4–8 m contribute very little to the total sediment yield at the outlet. In this study, sediment eroded in the upper part of the simulated area is largely deposited further down over the surface.

Effect of microtopography on internal erosion processes simulated by PSEM_2D

The 12 simulations of Table III performed for the 6% slope were run again with a plane surface of 6% slope to test the effect of the microrelief on the sediment yield and the internal erosion response. Figure 10 shows sediment yield versus slope length for the 6% slope with microrelief and the 6% plane slope. The results plotted are the average of 12 simulations. Sediment yield is overall larger for the plane surface at all positions along

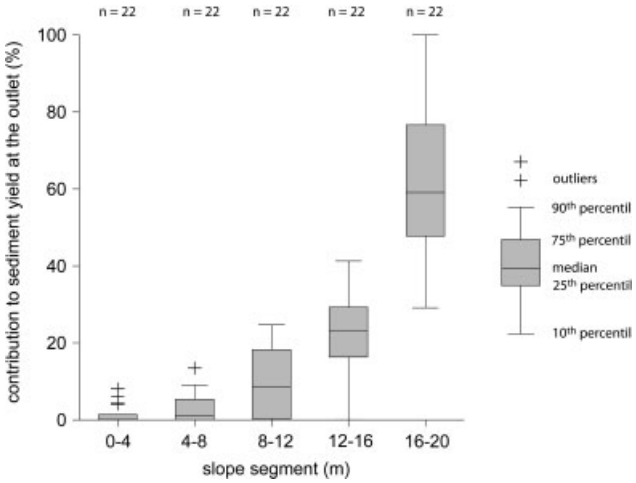

Figure 9. Range of contribution of five slope segments of 20 m^2 to the total sediment yield at the outlet of the simulated area

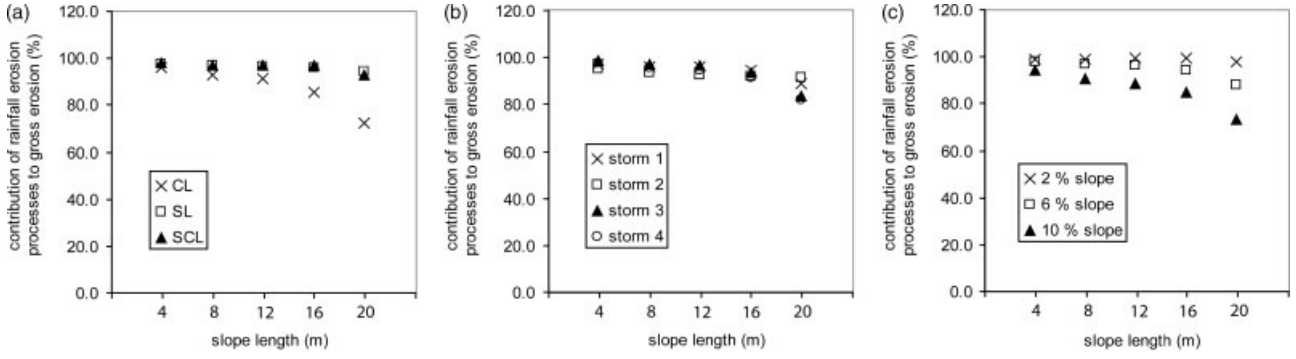

Figure 8. Contribution of rainfall erosion processes to gross erosion versus slope length. Results are grouped by (a) soil texture; (b) storm event and (c) slope gradient. Each point is the mean of 9 or 12 results

the slope. Different relationships between sediment yield and slope length were also simulated. The surface with microrelief displays a minimum at 8 m, an intermediate maximum at 4 m and a larger maximum at 20 m. Sediment transport capacity is low in the upper part of the simulated area. For a sudden increase in sediment transport capacity, the slope base, where flow in the rill network concentrates, has to be reached. However, the plane surface shows a continuous rise of sediment yield with slope length, which seems to tend towards an asymptote at the end of the slope. Such a spatial pattern is explained by the continuous increase in flow depth and, therefore, sediment transport capacity from the upstream border towards the base of the simulated area. The relationship between sediment yield simulated by the model and slope length is influenced by the microrelief of the surface. In this study, we do not reproduce the decrease in sediment yield with slope length that was observed by Parsons *et al*. (2006) in semi-arid conditions of Southern Arizona.

In the case of the plane surface, rainfall erosion produces approximately 100% of gross erosion over the entire simulated area and flow erosion is not activated. The regime is transport limited in these conditions. Figure 11 shows the contribution of five slope segments of 20 m^2 to the total sediment yield at the outlet of the simulated area for the 6% slope with microrelief and the 6% plane slope. Each point is the mean of seven results, since 5 of the 12 simulations for numerical tracing over the 6% slope with microrelief were excluded from the analysis for excessive divergence from the simulations without numerical tracing. The cause of the excessive divergence was not clear and could be related to model solution instability in a number of cases. The two surfaces show a major contribution of the lower part of the simulated area. However, in the case of the plane surface, all the segments contribute to the total sediment yield at the outlet of the simulated area and there is overall a more homogenous distribution of the contributions of the five slope segments. Resistance to sediment transport is very limited once particles are moved by runoff and conditions of transport are facilitated. However, for the slope with microrelief, the presence of rills may enable a threshold for the start of flow detachment to be overcome, but the increase in sediment yield with slope length occurs at a greater distance from the top of the simulated area. This result is supported by the intersection of the two curves in Figure 11.

Zhang *et al*. (2003) and Polyakov and Nearing (2004) worked with rare earth element oxides for tracing sediment in a 4 × 4 m laboratory plot set to a 10% slope and filled with a silty loam soil. The soil surface was gently packed to remove microrelief with a wood block. The plot area was subdivided into five 0·8-m strips stretching across the slope. Rainfall simulations of 1-h duration with constant rainfall intensity of 60 and 90 mm/h were performed. The authors found that the net soil loss was higher in the second and third strips (0·8–1·6 and 1·6–2·4 m). This, therefore, is different from the results

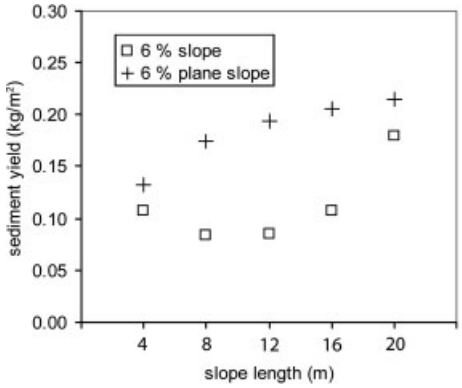

Figure 10. Sediment yield versus slope length for the 6% slope with microrelief and the 6% plane slope. Each point is the mean of 12 results

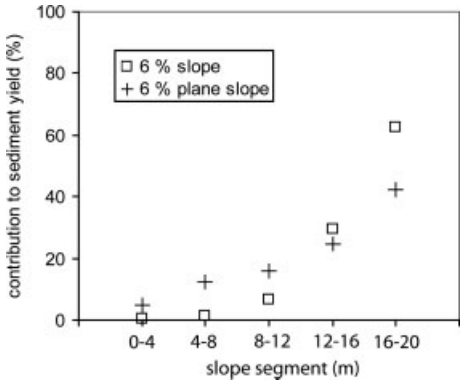

Figure 11. Contribution of five slope segments of 20 m^2 to the total sediment yield at the outlet of the simulated area for the 6% slope with microrelief and the 6% plane slope. Each point is the mean of seven results

plotted in Figures 9 and 11. The smaller length of their plot could explain the lesser role played by flow erosion in their case. Moreover, Polyakov and Nearing (2004) commented that the plot end controlled by the fixed elevation of the outlet funnel caused sediment accumulation on the lower slope position and therefore less erosion. In our results, if we exclude the results simulated for storm 2, which only causes runoff in the lower part of the simulated area, the four lower subplots contribute equally to the total sediment yield and the upper subplot has a lower contribution. In another study, Polyakov *et al*. (2004) applied a similar methodology at the sub-catchment scale (0·68 ha) and worked with natural rainfall events. The highest net soil losses came from the lower channels located close to the outlet. The channels showed a higher sediment delivery ratio than the backslopes and shoulder did, which was related to greater sediment transport efficiency in the channels than on the slopes. Therefore, our results are consistent with these observations. When slope length increases and microrelief plays a significant role in the development of a channel network, the contribution to total sediment yield of the areas with concentrated runoff increases. Furthermore, these areas control sediment export.

CONCLUSION

This study reports numerical simulation experiments that used PSEM_2D to investigate the interaction between internal processes of overland flow and erosion at the local scale and the determination of dominant processes as a function of soil length and changing environmental conditions. The results show that rainfall intensity is the variable that controls the amplitude of the runoff response, as explained by the selection of a Green and Ampt model for infiltration. In contrast, runoff is less sensitive to soil type and slope gradient in this study. Sediment yield at the outlet of the 100 m^2 simulated area correlates positively with rainfall intensity and slope gradient, but is less sensitive to soil type. Within the simulated area, sediment yield (soil loss per unit area) decreases overall with slope length in the upper part of the simulated area before increasing further downstream and reaching the highest values for a slope length of 20 m. On the upper part of the slope, the finer the particle diameter, the higher the sediment yield. However, at 20 m, shear stress of original soil (τ_{soil}) becomes more significant than particle diameter to explain sediment yield. Sediment yield is independent of slope length for the two temperate climate storms, whereas it increases with slope length for the Mediterranean climate storm. Higher runoff volume and flow discharge in this latter case produce higher sediment transport and activation of flow erosion. The contribution of rainfall erosion to gross erosion is dominant for all surfaces with slope lengths ranging from 4 to 20 m. The highest sediment yields correspond to cases where flow erosion is activated. Initiation of flow detachment appears more frequently between 12 and 16 m slope length, but an increase in slope gradient results in flow detachment starting upstream and causes an increase in the contribution of flow erosion. Sediment exported at the outlet of the simulated area comes predominantly from the subplot located near the outlet. In this study, microrelief and plane surface were also compared for the 6% slope. The results show that sediment yield is larger overall for the plane surface at all positions along the slope. The plane surface has different erosion patterns. Sediment yield increases with slope length and seems to tend towards an asymptote at the end of the slope. Rainfall erosion produces approximately 100% of gross erosion over the entire simulated area. Overall, there is more homogenous distribution of the contributions of the five slope segments to the total sediment yield at the outlet of the simulated area.

This study shows the relevance of using a fully coupled process-based model (infiltration-runoff-erosion) to understand the conditions that control sediment yield at different slope lengths. The role of microrelief in the development of a rill network that controls both the ratio between rainfall and flow erosion and the relationship between sediment yield and slope length is highlighted. There is a need for experimental, theoretical and modelling studies of overland flow hydraulics in a wide range of environmental conditions. Evaluation of the model against hydrology and erosion data with good spatial and temporal resolution is necessary, as well as comparison with other modelling approaches such as continuous deposition and transport distance concept.

ACKNOWLEDGEMENTS

The authors are grateful for the financial support provided by the Institut de Recherche pour le Développement (IRD), the French National Research Program on Hydrology (PNRH, INSU), the PROBASE (CGL2006-11619/HID) project and the Spanish Ministry of Science and Innovation (MICINN). Thanks are also due to the Physical and Regional Geography Research Group of the Department of Earth and Environmental Sciences of the K.U. Leuven and the Observatoire Hydro-météorologique Méditerranéen Cévennes-Vivarais (OHMCV) for making the rainfall data available. We would like to thank two anonymous referees for their constructive comments on an earlier version of this article.

NOTATION LIST

c	Volumetric sediment concentration, m^3/m^3
D_{rd}	Rate of disaggregation and redistribution of sediment by rain splash, $kg/m^2/s$
D_{rd_d}	Sediment detachment rate from original soil by rainfall, $kg/m^2/s$
D_{rd_rd}	Sediment redetachment rate from the deposited layer by rainfall, $kg/m^2/s$
D_{fd_d}	Detachment/deposition rate of sediment from original soil by runoff, $kg/m^2/s$
D_{fd_e}	Entrainment/deposition rate of sediment from the deposited layer by runoff, $kg/m^2/s$
D_{50}	Median sediment particle diameter, m
f	Darcy–Weisbach friction factor, (−)
h	Flow depth, m
h_f	Wetting front capillary pressure head, m
K_r	Flow erodibility parameter, s/m
K_s	Soil saturated hydraulic conductivity, m/s
l_d	Loose soil depth, m
q	Flow discharge per unit width in the flow direction, $m^3/s/m$
q_s	Sediment discharge per unit flow width in the flow direction, kg/m/s
R	Rainfall intensity, m/s
S_f	Energy slope, (−)
T_c	Sediment transport capacity of the flow, kg/m/s
u	Flow velocity in the x-direction, m/s
v	Flow velocity in the y-direction, m/s
$\overline{V}$	Depth-averaged flow velocity in the flow direction, m/s
V_f	Effective fall velocity, m/s
z_m	Maximum penetration depth of raindrop splash, m
α	Rainfall erodibility parameter for original soil, kg/m/mm

α_d Rainfall erodibility parameter for the deposited layer, kg/m/mm
θ_i Initial volumetric water content, (−)
θ_s Saturation volumetric water content, (−)
ε Percentage of a grid cell covered by a deposited layer of depth D_{50}, (−)
φ Raindrop-induced turbulence coefficient taken as 0·5 in this study, (−)
ρ_s Sediment particle density, kg/m^3
τ Flow shear stress in the flow direction, Pa
τ_c Critical shear stress of a spherical sediment particle, Pa
τ_{soil} Critical shear stress of original soil, Pa

REFERENCES

Abrahams AD, Li G, Parsons AJ. 1996. Rill hydraulics on a semiarid hillslope, Southern Arizona. *Earth Surface Processes and Landforms* **21**(1): 35–47.

Abrahams AD, Parsons AJ, Wainwright J. 1995. Controls and determination of resistance to overland flow on semiarid hillslopes, Walnut Gulch. *Journal of Soil and Water Conservation* **50**: 457–460.

Bennett JP. 1974. Concepts of mathematical modeling of sediment yield. *Water Resources Research* **10**(3): 485–492.

Brunton DA, Bryan RB. 2000. Rill network development and sediment budgets. *Earth Surface Processes and Landforms* **25**(7): 783–800.

Cerdan O, Poesen J, Govers G, Saby N, Le Bissonnais Y, Gobin A, Vacca A, Quinton JN, Auerswald K, Klik A, Kwaad F, Roxo MJ. 2006. Sheet and rill erosion. In *Soil Erosion in Europe*, Boardman J, Poesen J (eds). Wiley: Chichester; 501–513.

Chaplot V, Le Bissonnais Y. 2000. Field measurements of interrill erosion under different slopes and plot sizes. *Earth Surface Processes and Landforms* **25**(2): 145–153.

Elliot W, Liebenow A, Laflen J, Kohl K. 1989. *A Compendium of Soil Erodibility Data from Wepp Cropland Soil Field Erodibility Experiments 1987 and 1988*. NSERL Report 3, National Soil Erosion Research Laboratory, Agricultural Research Service, US Department of Agriculture: West Lafayette, Indiana. Available at ttp://topsoil.nserl.purdue.edu/nserlweb/weppmain/comp/comp.html [accessed 7th August 2008].

Esteves M, Faucher X, Galle S, Vauclin M. 2000. Overland flow and infiltration modelling for small plots during unsteady rain: numerical results versus observed values. *Journal of Hydrology* **228**(3): 265–282.

Favis-Mortlock DT. 1995. Validation of field-scale soil erosion models using common datasets. In *NATO Advanced Research Workshop on Global Change—Modelling Soil Erosion by Water*, Boardman J, Favis-Mortlock DT (eds). Springer-Verlag: Berlin, Oxford, England; 89–127.

Favis-Mortlock DT, Boardman J, Parsons AJ, Lascelles B. 2000. Emergence and erosion: a model for rill initiation and development. *Hydrological Processes* **14**: 2173–2205.

Foster GR, Meyer LD. 1972. A closed-form soil erosion equation for upland areas. In *Sedimentation Symposium to Honor Prof. H. A. Einstein*, vol. 12, Shen HW (ed). Colorado State University: Fort Collins; 12·1–12·19.

Foster GR, Flanagan DC, Nearing MA, Lane LJ, Risse LM, Finkner SC. 1995. *Ch. 11 Hillslope Erosion Component. Water Erosion Prediction Project: Hillslope Profile and Watershed Model Documentation*. NSERL Report 10, National Soil Erosion Research Laboratory, Agricultural Research Service, US Department of Agriculture, West Lafayette, Indiana.

Gilley JE, Flanagan DC, Kottwitz ER, Weltz MA. 1992. Darcy–Weisbach roughness coefficients for overland flow. In *Overland Flow Hydraulics and Erosion Mechanics*, Parsons AJ, Abrahams AD (eds). UCL Press: London; 25–51.

Giménez R, Govers G. 2001. Interaction between bed roughness and flow hydraulics in eroding rills. *Water Resources Research* **37**(3): 791–799.

Giménez R, Govers G. 2002. Flow detachment by concentrated flow on smooth and irregular bed. *Soil Science Society of America Journal* **66**: 1475–1483.

Govers G. 1992. Evaluation of transporting capacity formulae for overland flow. In *Overland Flow Hydraulics and Erosion Mechanics*, Parsons AJ, Abrahams AD (eds). UCL Press: London; 243–273.

Govers G, Poesen J. 1988. Assessment of the inter-rill and rill contributions to total soil loss from an upland field plot. *Geomorphology* **1**: 343–354.

Gumiere SJ, Le Bissonnais Y, Raclot D. 2009. Soil resistance to interrill erosion: model parameterization and sensitivity. *Catena* **77**(3): 274–284.

Hairsine PB, Rose CW. 1992. Modeling water erosion due to overland flow using physical principles. 1. Sheet flow. *Water Resources Research* **28**(1): 237–243.

Hairsine PB, Beuselinck L, Sander GC. 2002. Sediment transport through an area of net deposition. *Water Resources Research* **38**(6): 22-1–22-7.

Hairsine PB, Sander GC. 2009. Comment on 'a transport-distance based approach to scaling erosion rates': Parts 1, 2 and 3 by Wainwright, *et al*. *Earth Surface Processes and Landforms* **34**(6): 882–885.

Heng BCP, Sander GC, Scott CF. 2009. Modeling overland flow and soil erosion on nonuniform hillslopes: a finite volume scheme. *Water Resources Research* **45**: W05423, DOI:10.1029/2008WR007502.

Jetten V, de Roo A, Favis-Mortlock D. 1999. Evaluation of field-scale and catchment-scale soil erosion models. *Catena* **37**(3–4): 521–541.

Jetten V, Govers G, Hessel R. 2003. Erosion models: quality of spatial predictions. *Hydrological processes* **17**: 887–900.

Kinnell PIA. 2005. Raindrop impact induced erosion processes and prediction: a review. *Hydrological Processes* **19**(14): 2815–2844.

Knapen A, Poesen J, De Baets S. 2007a. Seasonal variations in soil erosion resistance during concentrated flow for a loess-derived soil under two contrasting tillage practices. *Soil and Tillage Research* **94**(2): 425–440.

Knapen A, Poesen J, Govers G, Gyssels G, Nachtergaele J. 2007b. Resistance of soils to concentrated flow erosion: a review. *Earth-Science Reviews* **80**(1–2): 75–109.

Lawrence DSL. 1997. Macroscale surface roughness and frictional resistance in overland flow. *Earth Surface Processes and Landforms* **22**: 365–382.

Leguédois S. 2003. *Mécanismes de l'érosion diffuse des sols. Modélisation du transfert et de l'évolution granulométrique des fragments de terre érodés*. PhD thesis, Université d'Orléans.

Leguédois S, Le Bissonnais Y. 2004. Size fractions resulting from an aggregate stability test, interrill detachment and transport. *Earth Surface Processes and Landforms* **29**: 1117–1129.

Leonard J, Richard G. 2004. Estimation of runoff critical shear stress for soil erosion from soil shear strength. *Catena* **57**(3): 233–249.

Michaelides K, Ibraim I, Nord G, Esteves M. 2010. Tracing sediment redistribution across a break in slope using rare earth elements. *Earth Surface Processes and Landforms*. http://dx.doi.org/10.1002/esp.1956.

Nearing MA, Norton LD, Bulgakov DA, Larionov GA, West LT, Dontsova KM. 1997. Hydraulics and erosion in eroding rills. *Water Resources Research* **33**(4): 865–876.

Nearing MA, Jetten V, Baffaut C, Cerdan O, Couturier A, Hernandez M, Le Bissonnais Y, Nichols MH, Nunes JP, Renschler CS. 2005. Modeling response of soil erosion and runoff to changes in precipitation and cover. *Catena* **61**(2–3): 131–154.

Nord G, Esteves M. 2005. PSEM_2D: a physically-based model of erosion processes at the plot scale. *Water Resources Research* **41**(8): W08407, DOI:10.1029/2004WR003690.

Nord G, Esteves M. 2007. Evaluation of sediment transport formulae and detachment parameters in eroding rills using PSEM_2D and the Water Erosion Prediction Project (WEPP) database. *Water Resources Research* **43**: W08420. DOI: 10.1029/2006WR005444.

Nord G, Esteves M, Lapetite J-M, Hauet A. 2009. Effect of particle density and inflow concentration of suspended sediment on bedload transport in rill flow. *Earth Surface Processes and Landforms* **34**(2): 253–263.

Parsons AJ, Abrahams AD, Luk S-H. 1991. Size characteristics of sediment in interrill overland flow on a semiarid hillslope, Southern Arizona. *Earth Surface Processes and Landforms* **16**: 143–152.

Parsons AJ, Brazier RE, Wainwright J, Powell DM. 2006. Scale relationships in hillslope runoff and erosion. *Earth Surface Processes and Landforms* **31**(11): 1384–1393.

Planchon O, Silvera N, Gimenez R, Favis-Mortlock D, Wainwright J, Le Bissonnais Y, Govers G. 2005. Estimation of flow velocity in a rill using an automated salt-tracing gauge. *Earth Surface Processes and Landforms* **30**: 833–844.

Polyakov VO, Nearing MA. 2004. Rare earth element oxides for tracing sediment movement. *Catena* **55**(3): 255–276.

Polyakov VO, Nearing MA, Shipitalo MJ. 2004. Tracking sediment redistribution in a small watershed: implications for agro-landscape evolution. *Earth Surface Processes and Landforms* **29**: 1275–1291.

Proffitt APB, Rose CW, Hairsine PB. 1991. Rainfall detachment and deposition: experiments with low slopes and significant water depths. *Soil Science Society of America Journal* **55**(2): 325–332.

Rawls WJ, Brakensiek DL, Miller N. 1983. Green-Ampt infiltration parameters from soils data. *Journal of Hydraulic Engineering-ASCE* **109**(1): 62–70.

Sander GC, Parlange JY, Barry DA, Parlange MB, Hogarth WL. 2007. Limitation of the transport capacity approach in sediment transport modeling. *Water Resources Research* **43**(2): W02403, DOI:10.1029/2006WR005177.

Scoging HM, Parsons AJ, Abrahams AD. 1992. Application of a dynamic overland flow hydraulic model to a semi-arid hillslope, Walnut Gulch, Arizona. In *Overland Flow Hydraulics and Erosion Mechanics*, Parsons AJ, Abrahams AD (eds). UCL Press: London; 105–145.

Song W, Liu PL, Yang MY, Xue YZ. 2003. Using REE tracers to measure sheet erosion changing to rill erosion. *Journal of Rare Earths* **21**(5): 587–590.

Tatard L, Planchon O, Wainwright J, Nord G, Favis-Mortlock D, Silvera N, Ribolzi O, Esteves M, Huang CH. 2008. Measurement and modelling of high-resolution flow-velocity data under simulated rainfall on a low-slope sandy soil. *Journal of Hydrology* **348**(1–2): 1–12.

Van Oost K, Govers G, Cerdan O, Thauré D, Van Rompaey A, Steegen A, Nachtergaele J, Takken I, Poesen J. 2005. Spatially distributed data for erosion model calibration and validation: the Ganspoel and Kinderveld datasets. *Catena* **61**(2–3): 105–121.

Wainwright J, Parsons AJ. 2002. The effect of temporal variations in rainfall on scale dependency in runoff coefficients. *Water Resources Research* **38**(12): 7-1–7-10.

Wainwright J, Parsons AJ, Muller EN, Brazier RE, Powel DM, Fenti B. 2008a. A transport-distance approach to scaling erosion rates: I. Background and model development. *Earth Surface Processes and Landforms* **33**(5): 813–826.

Wainwright J, Parsons AJ, Müller EN, Brazier RE, Powell DM, Fenti B. 2008b. A transport-distance approach to scaling erosion rates: 2. Sensitivity and evaluation of MAHLERAN. *Earth Surface Processes and Landforms* **33**(6): 962–984.

Wainwright J, Parsons AJ, Muller EN, Brazier RE, Powell DM, Fenti B. 2008c. A transport-distance approach to scaling erosion rates: 3. Evaluating scaling characteristics of MAHLERAN. *Earth Surface Processes and Landforms* **33**(7): 1113–1128.

Zhang XC, Nearing MA, Polyakov VO, Friedrich JM. 2003. Using rare-earth oxide tracers for studying soil erosion dynamics. *Soil Science Society of America Journal* **67**: 279–288.

